(Received 10 January 2024, Accepted 3 February 2024, Scheduled 17 February 2024)

Finite-Control-Set Model Predictive Current Closed-Loop Control Based on Prediction Error Compensation for PMSM

Wenxuan Luo[1] and Zhun Cheng[2,*]

[1] International Education Institute, North China Electric Power University, Baoding 071003, China
[2] Hunan Railway Professional Technology College, Zhuzhou 412001, China

ABSTRACT: Finite-control-set model predictive control (FCS-MPC) for permanent magnet synchronous motors (PMSMs) has attracted attention due to its better theoretical performance. However, as motor operating conditions change, motor parameter mismatch can lead to intolerable prediction errors which significantly deteriorate stator current harmonics and torque ripples. To solve this issue, a finite-control-set model predictive current closed-loop control strategy is proposed. First, based on the analysis of the prediction equations, the voltage-independent and voltage-dependent parts of the prediction errors are separated. Secondly, according to the different features of prediction errors caused by zero and non-zero vectors, the decoupling of the two parts of prediction error is realized. And PI controllers are introduced to observe the two different types of DC components respectively to make the observation more stable and accurate. Thirdly, feedback compensation is performed to modify the prediction equations. With the design of model predictive current closed-loop control, the prediction error quickly converges to the minimum. Finally, the experimental outcomes prove the effectiveness of this strategy.

1. INTRODUCTION

PMSM has bright prospects in lots of fields such as electric vehicles and rail metros due to its wide speed range, high air-gap flux density, etc. [1–5]. The classical control strategies are field-oriented control (FOC) strategy and direct torque control (DTC) strategy [6, 7]. The FOC strategy based on orienting the rotor magnetic field direction, using coordinate transformation to separate the direct and quadrature axes, combined with classical PI controller, achieves a good steady-state performance. The DTC strategy directly controls the torque and stator flux magnitude using a switching table, resulting in a degradation of steady state performance, but a fast dynamic response [8, 9].

Model Predictive Control (MPC) has the advantages of multi-objectives, multi-constraints, high closed-loop bandwidth, and simple structure [10, 11]. Upon the state of the control set, MPC can be sorted into two types: finite-control-set and continuous-control-set model predictive control (FCS-MPC and CCS-MPC). Depending on control objectives, MPC can be further categorized into predictive current, torque, and flux control. Among them, finite-control-set model predictive current control (FCS-MPCC) combining FSC-MPC and current control strategy has been widely studied due to its simplicity and without weighting factor [12]. With stator current as the prediction variable, FCS-MPCC strategy obtains future current under the action of a finite number of eight discrete voltage vectors. Then the voltage vector that has the lowest cost function is chosen. Both FCS-MPCC and FOC aim at current control, but FCS-MPCC eliminates the need for cumbersome voltage modulation, removes the use of current regulator, and boosts the dynamic response [13]. The similarity between FCS-MPCC and DTC strategy mechanisms is that both aim at selecting the optimal voltage vector and both have a fast dynamic response, but FCS-MPCC selects the vectors on a sufficient and accurate basis, so the steady state performance is better [14].

Despite the theoretical advantages of FSC-MPCC, the control effect relies on the accuracy of motor parameters and other factors. In practice, motor parameters are difficult to be measured accurately and will change with various working conditions [15]. If there is no current prediction correction part, this control strategy is open-loop predictive control. For open-loop predictive control, parameter mismatch can cause an obvious difference between prediction value and actual value, then affect performance of system.

Currently, scholars have proposed many algorithms to reduce the effects of parameter mismatch in MPC. These algorithms include estimation and compensation of perturbations, model-free prediction, online parameter identification, etc. [16], record the prediction error resulting from each voltage vector in each cycle, and compensate the corresponding predicted value. However, as all voltage vectors are applied intermittently during motor operation, this approach has the issue of stagnant prediction error updating. Based on [16, 17], update the current prediction error resulting from each voltage vector simultaneously in one control cycle. However, the motor parameters are used in its calculation process, and the inaccuracy of the parameters can also introduce error. In [18], integrating prediction error yields lumped disturbance, then the disturbance is compensated in real time. Therefore, the partial correction of the prediction equation reduces the current prediction error. In [19] and [20], the perturbation-related parameters are directly calculated based on information such as voltage and current prediction errors at past moments, and the modi-

* Corresponding author: Zhun Cheng (120277982@qq.com).

fied prediction equations are updated during each sampling period. However, the direct calculation method is sensitive to external disturbances and measurement errors, which can affect the effectiveness of the compensation. In [21], a model self-regulation technique was presented to calculate the coefficient variation values by using the information of three control cycles and to design the integral estimation method to correct each coefficient of the prediction equations in real time. However, the matrix containing the information of three cycles may be irreversible, which leads to inaccurate calculations.

In addition to the idea of integration, the disturbance observer is also a well-known strategy for compensating the lumped disturbance. The basic principle of the lumped disturbance compensation observation [22–26] is to treat the errors from all influencing factors such as motor parameter mismatch, external disturbances, measurement errors, and inverter nonlinearities as a lumped disturbance, estimating this disturbance by designing an observation mechanism, and then realizing real-time compensation using this estimated disturbance. In [22], a novel strategy is introduced, amalgamating a disturbance observer with a sliding mode (SM) exponential reaching law and deadbeat predictive current control. This approach involves real-time compensation of observed disturbances to the prediction equation, effectively minimizing current prediction errors. By taking parameter mismatches into consideration as a lumped disturbance and state variables, an improved extended state observer (ESO) was developed in [23]. This advancement serves to further elevate the performance of the SM disturbance observer. In [24], a deadbeat control strategy is introduced, incorporating an improved mathematical model and an exponential ESO for observation of lumped disturbance. In [25], an enhanced deadbeat MPCC, combining multiple disturbance observers, is introduced. This approach integrates the Generalized PI Observer (GPIO) and SM observer (SMO). In this system, the SMO is utilized to minimize the build-up period due to higher-order GPIO, while GPIO effectively tracks disturbances. In [26], an innovative model-free deadbeat MPCC approach is introduced, leveraging a Luenberger disturbance observer. The method estimates the system's lumped disturbance by using the observer without motor parameters. However, lumped disturbance compensation approach is not effective to FSC-MPCC, for reasons that will be analyzed later.

A closed-loop control strategy for FSC-MPCC is presented to produce high-performance current tracking effect by reducing prediction error. First, the components of the error due to parameter mismatch are analyzed. Then, the reason that the method of the lumped disturbance compensation is not applicable to FCS-MPC is analyzed. Furthermore, by reasonably categorizing the prediction error into two types and introducing stable proportional-integral (PI) controllers to observe the corresponding parts of the error in a decoupled way, the closed-loop control is designed to minimize the current prediction error. Finally, the experimental outcomes proved that the method in this paper is accurate and efficient.

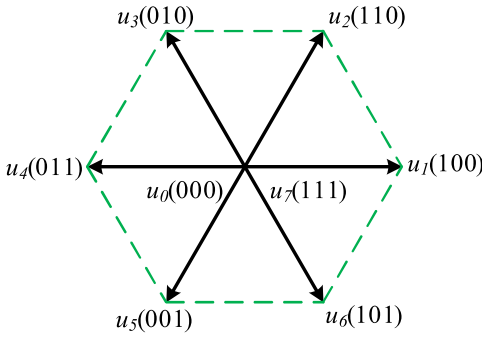

FIGURE 1. Voltage vectors diagram.

2. BASIC FSC-MPCC THEORY AND ANALYSIS OF PREDICTION ERROR

2.1. Basic FSC-MPCC Theory in PMSM

The inverter can generate a total of eight combinations of switching states. The voltage vectors are shown in Fig. 1.

The current dynamic equation of PMSM in the d-q frame is expressed as

$$\begin{cases} \frac{d}{dt} i_d = -\frac{R_s}{L_d} i_d + \frac{L_q}{L_d} \omega_e i_q + \frac{1}{L_d} u_d \\ \frac{d}{dt} i_q = -\frac{R_s}{L_q} i_q - \frac{L_d}{L_q} \omega_e i_d - \frac{\psi_f}{L_q} \omega_e + \frac{1}{L_q} u_q \end{cases} \tag{1}$$

where R_s is the motor stator resistance; L_d and L_q are the *dq*-axis components of stator inductance, respectively; ψ_f is the rotor permanent magnet flux linkage; ω_e is the electrical rotor angular velocity; i_d and i_q are the *dq*-axis components of stator current, respectively; u_d and u_q are the *dq*-axis components of stator voltage, respectively.

By the forward Euler method, Eq. (1) is discretized as

$$\begin{cases} i_d^p(k+1) = i_d(k) - \frac{T_s R_s}{L_d} i_d(k) + \frac{T_s L_q}{L_d} \omega_e(k) i_q(k) \\ \qquad + \frac{T_s}{L_d} u_d(k) \\ i_q^p(k+1) = i_q(k) - \frac{T_s R_s}{L_q} i_q(k) - \frac{T_s L_d}{L_q} \omega_e(k) i_d(k) \\ \qquad - \frac{T_s \psi_f}{L_q} \omega_e(k) + \frac{T_s}{L_q} u_q(k) \end{cases} \tag{2}$$

where T_s is the sampling period.

In practical digital circuits, the chosen voltage vector is delayed until the subsequent cycle. Therefore, a two-step prediction is employed, utilizing Eq. (2) once more to forecast current values at the $(k+2)$th moment. Furthermore, constraints are included in cost function to prevent the stator current from going beyond the maximum transient current ($i_{\max}$), as shown in Eq. (3). The predicted values for the $(k+2)$th moment corresponding to eight voltage vectors are calculated. Then, by substituting the predicted values into Eq. (3), the voltage vector that minimizes Eq. (3) is selected.

$$\begin{cases} g = |i_d\_ref - i_d^p(k+2)|^2 + |i_q\_ref - i_q^p(k+2)|^2 \\ \qquad + I_{\lim}(k+2) \\ I_{\lim}(k+2) = \begin{cases} 0 & \text{if } |i(k+2)| \le |i_{\max}| \\ \infty & \text{if } |i(k+2)| > |i_{\max}| \end{cases} \\ |i(k+2)| = \sqrt{i_d^p(k+2)^2 + i_q^p(k+2)^2} \end{cases} \tag{3}$$

where i_d_ref and i_q_ref represent the reference values for *dq*-axis stator current components, respectively.

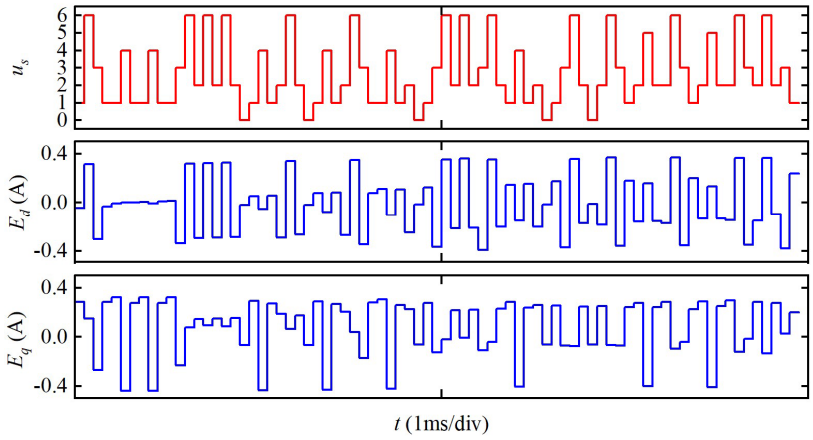

FIGURE 2. Stator current predictive error for FSC-MPCC when parameter mismatch. The numbers 0–6 of u_s represent 7 different voltage vectors.

2.2. Analysis of Current Prediction Error

From Eq. (2), the accuracy of current prediction values relies on the error among the motor parameters (R_s, L_d, L_q, ψ_f) employed in the prediction algorithm and the actual motor parameters. The motor parameters vary during the operation of motor, leading to an error between prediction value and actual value. Besides parameter mismatch as a factor, other unmodeled disturbances also contribute to the current prediction error. Considering all disturbances, the actual stator current prediction equation is rewritten as

$$\begin{cases} i_d(k+1) = i_d(k) - \frac{T_s\tilde{R}_s}{\tilde{L}_d} i_d(k) + \frac{T_s\tilde{L}_q}{\tilde{L}_d}\omega_e(k)i_q(k) \\ \qquad\qquad + \frac{T_s}{\tilde{L}_d} u_d(k) + h_d \\ i_q(k+1) = i_q(k) - \frac{T_s\tilde{R}_s}{\tilde{L}_q} i_q(k) - \frac{T_s\tilde{L}_d}{\tilde{L}_q}\omega_e(k)i_d(k) \\ \qquad\qquad - \frac{T_s\tilde{\psi}_f}{\tilde{L}_q}\omega_e(k) + \frac{T_s}{\tilde{L}_q} u_q(k) + h_q \end{cases} \tag{4}$$

where h_d and h_q are the *dq*-axis components of current prediction error due to other unmodeled disturbances, respectively; $\tilde{R}_s$, $\tilde{L}_d$, $\tilde{L}_q$, $\tilde{\psi}_f$ are the true values of the stator resistance, the *dq*-axis stator inductance components, and the rotor permanent magnet flux linkage, respectively.

By subtracting Eq. (2) from Eq. (4), the *dq*-axis components of current prediction error at the $(k+1)$th moment can be obtained as follows:

$$\begin{cases} E_d(k+1) = i_d(k+1) - i_d^p(k+1) \\ \qquad\qquad = D_1 + h_d + A_3u_d(k) \\ E_q(k+1) = i_q(k+1) - i_q^p(k+1) \\ \qquad\qquad = D_2 + h_q + B_4u_q(k) \\ D_1 = A_1i_d(k) + A_2\omega_e(k)i_q(k) \\ D_2 = B_1i_q(k) + B_2\omega_e(k)i_d(k) + B_3\omega_e(k) \\ A_1 = T_s\left(\frac{R_s}{L_d} - \frac{\tilde{R}_s}{\tilde{L}_d}\right),\ A_2 = T_s\left(\frac{\tilde{L}_q}{\tilde{L}_d} - \frac{L_q}{L_d}\right), \\ A_3 = T_s\left(\frac{1}{\tilde{L}_d} - \frac{1}{L_d}\right) \\ B_1 = T_s\left(\frac{R_s}{L_q} - \frac{\tilde{R}_s}{\tilde{L}_q}\right),\ B_2 = T_s\left(\frac{L_d}{L_q} - \frac{\tilde{L}_d}{\tilde{L}_q}\right), \\ B_3 = T_s\left(\frac{\psi_f}{L_q} - \frac{\tilde{\psi}_f}{\tilde{L}_q}\right),\ B_4 = T_s\left(\frac{1}{\tilde{L}_q} - \frac{1}{L_q}\right) \end{cases} \tag{5}$$

Compared to very short sampling interval, the motor parameters change slowly and can be regarded as constants. Thus, coefficients $A_{1\sim3}$ and $B_{1\sim4}$, which depend on the motor parameters, can be considered as constants. h_d and h_q can also be considered as constants due to their small variations. From Eq. (5), the current prediction errors are linked to the *dq*-axis current components, electrical angular velocity, as well as *dq*-axis voltage components. During the steady-state condition, i_d, i_q, and ω_e can be regarded as invariants, so the D_1 and D_2 error parts can also be regarded as constants. During the dynamic operating condition, the D_1 and D_2 error parts are caused by the current and electrical angular velocity transitioning from one steady-state values to another. For FSC-MPCC, a voltage vector is employed for a sampling period, and the amplitudes of u_d and u_q vary over a wide range (from $-2*U_{dc}/3$ to $2*U_{dc}/3$). Due to the discrete nature of individual voltage vector, u_d and u_q are non-differentiable quantities in time and discontinuously vary (e.g., one active vector is selected in the previous moment which has large values of u_d and u_q, and one zero vector in the next moment, which has both u_d and u_q as 0). Therefore, similar to u_d and u_q, the voltage-dependent error components (A_3u_d and B_4u_q) vary over a wide range and are discontinuously nondifferentiable during steady-state and dynamic operating conditions. Moreover, since the voltage-dependent error is the main part of the prediction error, the prediction errors E_q and E_d are also quantities with a large range of variation and discontinuous non-differentiable, as shown in Fig. 2.

From Fig. 2, the current prediction errors vary both positively and negatively over a broad range with different voltage vectors. Treating the prediction errors as a lumped disturbance, the approach of observing the disturbance using an observer or to integrate the current prediction errors to get the disturbance value and then compensate for them can only address the DC components of the prediction errors, not the components that vary with voltage. Consequently, substantial errors may still persist even after the lumped disturbance compensation.

3. THE PROPOSED METHOD

Since traditional FSC-MPCC is an open-loop predictive control, the predictive model cannot be effectively adjusted when

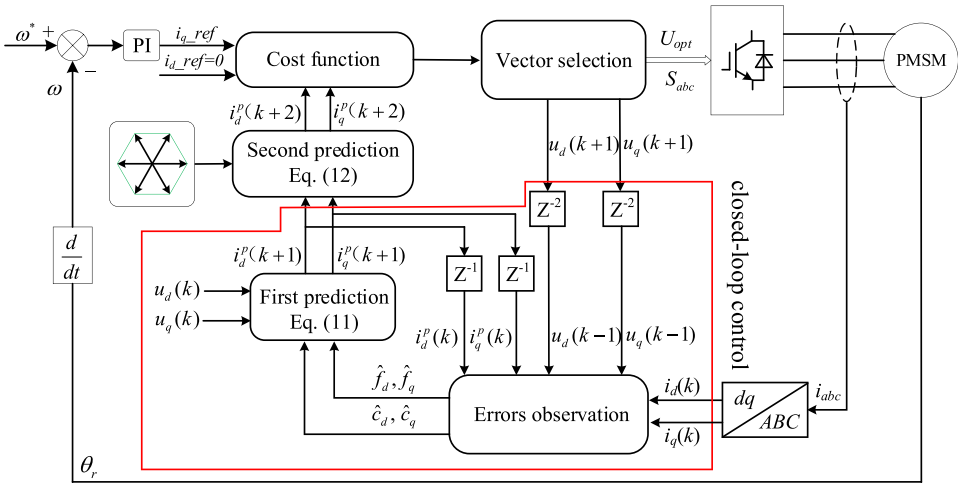

FIGURE 3. The block diagram of the proposed method.

motor parameters used in prediction equation are mismatched with actual motor parameters. From above analysis of prediction error, it is clear that the lumped disturbance compensation approach is hard to reach the expected performance. Therefore, the method in this paper considers the discrete nature of voltage vectors, divides the prediction error into voltage-dependent and voltage-independent error parts, and introduces PI controllers to obtain the error values of voltage-independent part and the coefficients of the voltage-dependent part, and then carries out the feedback compensation, which constructs the closed-loop FSC-MPCC strategy. The block diagram is shown in Fig. 3.

The voltage-independent error terms in Eq. (5) are denoted as f_d and f_q, respectively, and the voltage coefficients of the voltage-dependent error terms are denoted as c_d and c_q (i.e., $c_d = A_3$, $c_q = B_4$). The current prediction error equation can be rewritten as follows:

$$\begin{cases} E_d(k+1) = i_d(k+1) - i_d^p(k+1) = f_d + c_d u_d(k) \\ E_q(k+1) = i_q(k+1) - i_q^p(k+1) = f_q + c_q u_q(k) \\ f_d = D_1 + h_d = A_1 i_d(k) + A_2 \omega_e(k) i_q(k) + h_d \\ f_q = D_2 + h_q = B_1 i_q(k) + B_2 \omega_e(k) i_d(k) \\ \qquad + B_3 \omega_e(k) + h_q \end{cases} \tag{6}$$

By adding Eq. (2) and Eq. (6), the discrete current equation for PMSM is expressed as follows:

$$\begin{cases} i_d(k+1) = \left[i_d(k) - \frac{T_s R_s}{L_d} i_d(k) + \frac{T_s L_q}{L_d} \omega_e(k) i_q(k) \right. \\ \qquad \left. + \frac{T_s}{L_d} u_d(k) \right] + f_d + c_d u_d(k) \\ i_q(k+1) = \left[i_q(k) - \frac{T_s R_s}{L_q} i_q(k) - \frac{T_s L_d}{L_q} \omega_e(k) i_d(k) \right. \\ \qquad \left. - \frac{T_s \psi_f}{L_q} \omega_e(k) + \frac{T_s}{L_q} u_q(k) \right] + f_q + c_q u_q(k) \end{cases} \tag{7}$$

The components of f_d and f_q are D_1, h_d and D_2, h_q, respectively. From the previous analysis, D_1 and D_2 can be regarded as constants during steady state, so f_d and f_q can also be constants. With variations in motor speed and load torque, the motor changes its output electromagnetic torque and enters another steady state after a short adjustment. In this process, f_d and f_q also transition from one steady constant value to another. c_d and c_q are constants related to inductance mismatch. For the introduced PI controllers, both types of DC information are observable.

From Eq. (6), the prediction errors E_q and E_d contain the information of f_d, f_q, c_d and c_q. When the optimal voltage vector applied at the $(k-1)$th moment is a zero vector, the prediction error measured at the kth moment does not contain any voltage term, and the current errors E_q and E_d at the kth instant have a direct relationship with f_d and f_q. Therefore, based on the premise of applying a zero vector at the $(k-1)$th moment, the PI controllers can be designed to observe f_d and f_q, as shown in Eq. (8). The control schematic is shown in Fig. 4.

$$\begin{cases} \hat{f}_d(k) = I_d(k) + K_{d1}(i_d(k) - i_d^p(k)) \\ I_d(k) = I_d(k-1) + T_s G_{d1}(i_d(k) - i_d^p(k)) \\ \hat{f}_q(k) = I_q(k) + K_{q1}(i_q(k) - i_q^p(k)) \\ I_q(k) = I_q(k-1) + T_s G_{q1}(i_q(k) - i_q^p(k)) \end{cases} \tag{8}$$

The observed f_d and f_q are feedback compensated into the prediction equation, and the compensated current prediction equation is as follows:

$$\begin{cases} i_d^p(k+1) = \left[i_d(k) - \frac{T_s R_s}{L_d} i_d(k) + \frac{T_s L_q}{L_d} \omega_e(k) i_q(k) \right. \\ \qquad \left. + \frac{T_s}{L_d} u_d(k) \right] + \hat{f}_d \\ i_q^p(k+1) = \left[i_q(k) - \frac{T_s R_s}{L_q} i_q(k) - \frac{T_s L_d}{L_q} \omega_e(k) i_d(k) \right. \\ \qquad \left. - \frac{T_s \psi_f}{L_q} \omega_e(k) + \frac{T_s}{L_q} u_q(k) \right] + \hat{f}_q \end{cases} \tag{9}$$

When an active voltage vector is applied at the $(k-1)$th moment, and both $u_d(k-1)$ and $u_q(k-1)$ are not zero, the prediction errors E_q and E_d contain the voltage-independent components and voltage-dependent components from Eq. (6). However, since f_d and f_q have been compensated into the prediction equation by the zero-vector case, E_q and E_d do not contain f_d

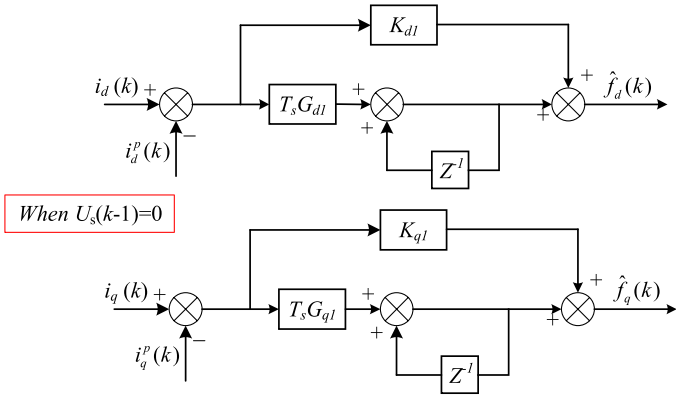

FIGURE 4. Control schematic for proportional integral controllers to observe f_d and f_q.

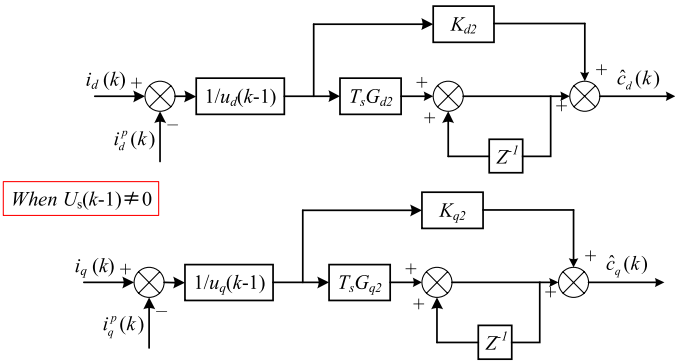

FIGURE 5. Control schematic for proportional integral controllers to observe c_d and c_q.

and f_q, so E_d/u_d and E_q/u_q have a direct logical relationship with c_d and c_q. Therefore, based on the premise that an active vector is applied at the $(k-1)$th moment, and both $u_d(k-1)$ and $u_q(k-1)$ are not zero. The PI controllers can be designed to observe c_d and c_q as in Eq. (10), and the control schematic is shown in Fig. 5.

$$\begin{cases} \Delta c_d = \frac{i_d(k)-i_d^p(k)}{u_d(k-1)},\ \hat{c}_d(k) = V_d(k) + K_{d2}\Delta c_d, \\ V_d(k) = V_d(k-1) + T_sG_{d2}\Delta c_d \\ \Delta c_q = \frac{i_q(k)-i_q^p(k)}{u_q(k-1)},\ \hat{c}_q(k) = V_q(k) + K_{q2}\Delta c_q, \\ V_q(k) = V_q(k-1) + T_sG_{q2}\Delta c_q \end{cases} \tag{10}$$

In Eq. (8) and Eq. (10), K_{d1}, K_{q1}, G_{d1}, G_{q1} and K_{d2}, K_{q2}, G_{d2}, G_{q2} are the observer parameters. To ensure the stability of this closed-loop feedback system and obtain a good dynamic and steady-state response, it is important to choose the appropriate parameters. The process of tuning the parameters is relatively simple and will not be discussed here.

Since only one voltage vector is applied in one sampling period, only one set of data, f_d, f_q, or c_d, c_q, is updated in a control cycle, and the data that has not been updated follows the latest value. Since both f_d, f_q and c_d, c_q can be regarded as constants at steady state, the delayed update causes little impact on the compensation accuracy. After feedback compensation into the prediction equation, the current prediction equation is as follows:

$$\begin{cases} i_d^p(k+1) = \left[i_d(k) - \frac{T_sR_s}{L_d}\, i_d(k) + \frac{T_sL_q}{L_d}\, \omega_e(k) i_q(k) \right. \\ \qquad \left. + \frac{T_s}{L_d}\, u_d(k)\right] + \hat{f}_d + \hat{c}_d u_d(k) \\ i_q^p(k+1) = \left[i_q(k) - \frac{T_sR_s}{L_q}\, i_q(k) - \frac{T_sL_d}{L_q}\, \omega_e(k) i_d(k) \right. \\ \qquad \left. - \frac{T_s\psi_f}{L_q}\, \omega_e(k) + \frac{T_s}{L_q}\, u_q(k)\right] + \hat{f}_q + \hat{c}_q u_q(k) \end{cases} \tag{11}$$

Considering two-step prediction, after the first step of current prediction, the second step of prediction is formulated as Eq. (12).

$$\begin{cases} i_d^p(k+2) = \left[i_d(k+1) - \frac{T_sR_s}{L_d}\, i_d(k+1) \right. \\ \qquad \left. + \frac{T_sL_q}{L_d}\, \omega_e(k) i_q(k+1) + \frac{T_s}{L_d}\, u_d(k+1)\right] \\ \qquad + \hat{f}_d + \hat{c}_d u_d(k+1) \\ i_q^p(k+2) = \left[i_q(k+1) - \frac{T_sR_s}{L_q}\, i_q(k+1) \right. \\ \qquad - \frac{T_sL_d}{L_q}\, \omega_e(k) i_d(k+1) - \frac{T_s\psi_f}{L_q}\, \omega_e(k) \\ \qquad \left. + \frac{T_s}{L_q}\, u_q(k+1)\right] + \hat{f}_q + \hat{c}_q u_q(k+1) \end{cases} \tag{12}$$

In this paper, the prediction equations and prediction error are analyzed in detail. Then the values of f_d, f_q, c_d, and c_q are observed, and the observed values are fed back to correct the prediction equations. This closed-loop prediction method is used instead of the open-loop prediction method to improve the immunity and robustness of the inner loop of current prediction. In the following, experiments will be performed to verify that the proposed method can eliminate the prediction error in time and improve the robustness of the system under the parameter mismatch.

4. EXPERIMENTAL VERIFICATION

This paper is based on RT-LAB experimental platform for experimental verification, and the platform is shown in Fig. 6. To highlight the effectiveness of the method proposed in this paper, the traditional FCS-MPCC (T-MPCC) and lumped disturbance compensation FCS-MPCC (LDC-MPCC) [22] are used as comparison experiments in this paper, and the sampling frequency is 40 kHz. i_{q_ref} is derived from the speed loop PI controller, and i_{d_ref} is 0 A. The parameters of the PI controllers are set as $K_{d1} = K_{q1} = 0.05$, $G_{d1} = G_{q1} = 500$, and $K_{d2} = K_{q2} = 0.02$, $G_{d2} = G_{q2} = 200$. The surface-mounted PMSM parameters are shown in Table 1.

Here, R_{s0}, L_{s0}, and ψ_{f0} are nominal values, and R_s, L_s, and ψ_f are the parameters that are used in prediction equation.

Since the change of motor parameters is not controlled, this paper simulates motor parameters mismatch by changing the

Symbol	Description	Value
U_N (V)	DC link voltage	310
N (rpm)	Rated speed	2000
T_N (N·m)	Rated torque	6
P_n	pole pairs	4
R_{s0} (Ω)	Stator resistance	1.2
L_{s0} (mH)	Synchronous inductance	8.5
ψ_{f0} (Wb)	Flux linkage	0.175
J (kg·m^2)	Motorinertia	0.00275

TABLE 1. Parameters.

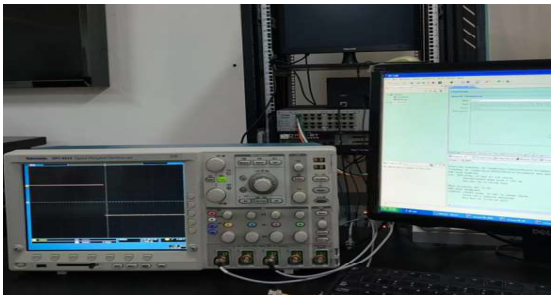

FIGURE 6. Experimental platform.

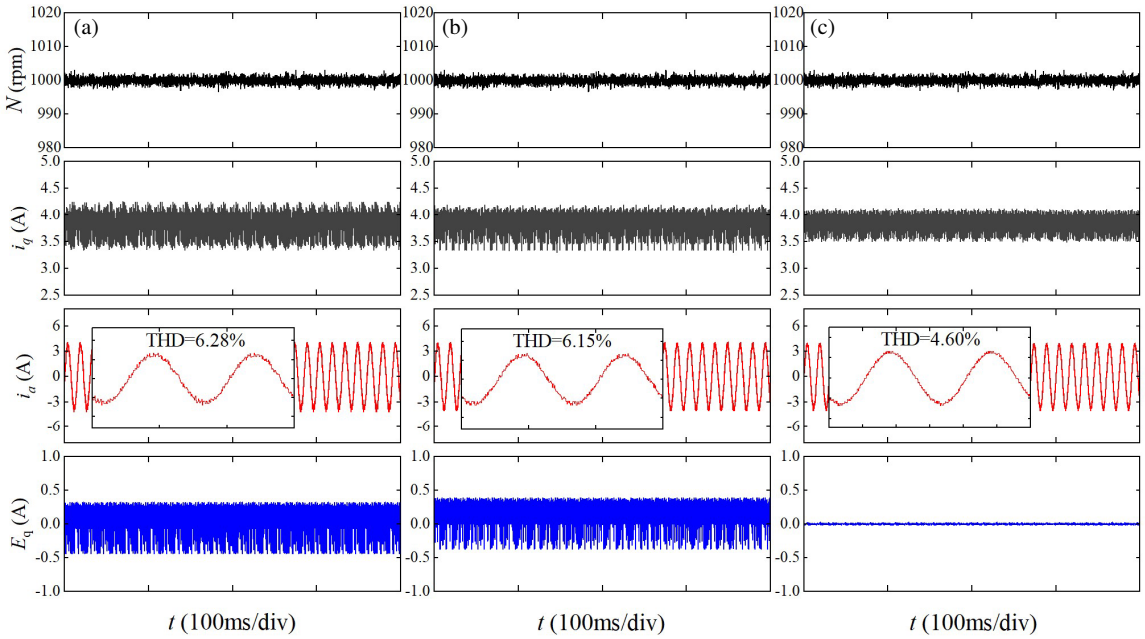

FIGURE 7. Steady-state experimental results: motor speed N, i_q, i_a and E_q of three methods at 1000 rpm and 4 Nm load torque when $R_s = 0.2R_{s0}$, $L_s = 3L_{s0}$ and $\psi_f = 2\psi_{f0}$. (a) T-MPCC. (b) LDC-MPCC. (c) The proposed method.

values of the parameters used in the current prediction equation. Three control methods are compared and experimented under stable operating condition when all three parameters are severely mismatched. The results are shown in Fig. 7, where the parameters used in the prediction calculations satisfy $R_s = 0.2R_{s0}$, $L_s = 3L_{s0}$, and $\psi_f = 2\psi_{f0}$; the motor speed is 1000 rpm; and the load torque is 4 Nm.

As shown in Figs. 7(a) and (b), when there is a mismatch in parameters, the q-axis current prediction errors of both the T-MPCC and LDC-MPCC are very large, with the maximal errors being 0.42 A and 0.38 A, respectively. Compared to T-MPCC, LDC-MPCC compensates the DC disturbance so that the positive and negative magnitudes of the errors are the same, slightly reducing the maximum error. The lumped disturbance compensation method can only eliminate the DC component of the disturbance, but not the prediction error related to voltage. In Fig. 7(c), the proposed method converges the current prediction error E_q to within ± 0.03 A by effective compensation, which improves the prediction accuracy. Substantial q-axis current steady-state ripples and stator current harmonics result from the substantial prediction errors of T-MPCC and LDC-MPCC. The i_q ripples reach 0.93 A and 0.86 A, and the stator current harmonics are 6.28% and 6.15%, respectively. The proposed scheme effectively reduces the current prediction error, resulting in a decrease of i_q ripples and stator current harmonics to 0.62 A and 4.60%, respectively.

Based on the steady-state experiments mentioned above, the experiments of sudden change of motor speed reference and load torque are added for the proposed method, and the results are shown in Fig. 8. In Fig. 8(a), when the motor speed changes (1000 rpm $\rightarrow$ 1500 rpm $\rightarrow$ 1000 rpm $\rightarrow$ -1000 rpm), the proposed method can keep the prediction error in a very small range, and the experimental results show that the dynamics also do not affect the accuracy of the proposed method's observation. In Fig. 8(b), the motor load torque changes (2 Nm $\rightarrow$ 4 Nm $\rightarrow$ 6 Nm $\rightarrow$ 3 Nm). A similar conclusion can be drawn that, with different loads or sudden loading and unloading, the proposed method can keep the prediction error in a very small range.

In order to verify the dynamic regulation ability of proposed method, the motor parameters used in the prediction equation are changed suddenly when the motor speed is 1000 rpm with

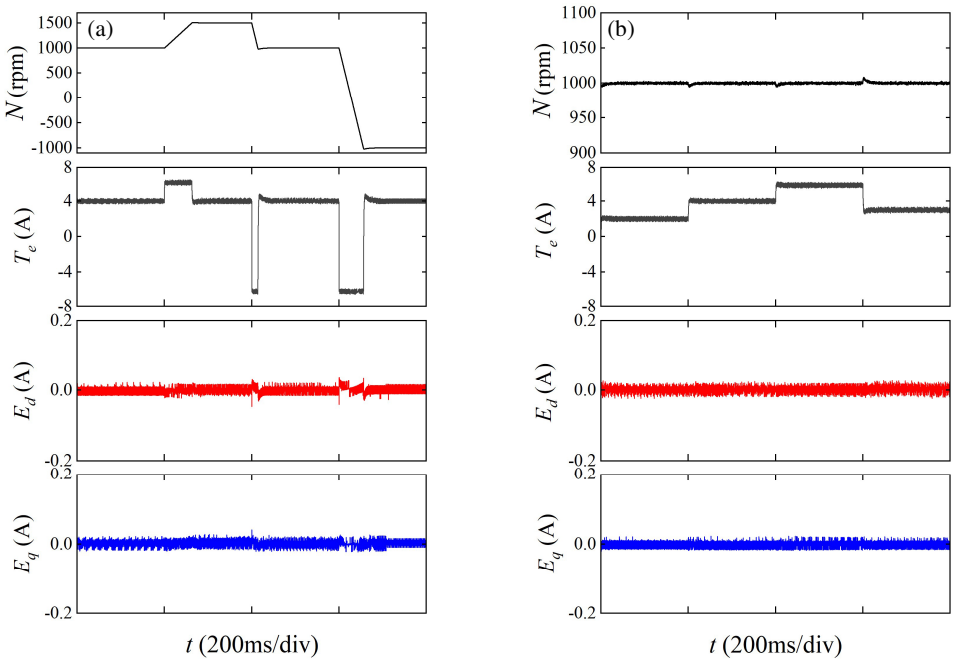

FIGURE 8. Dynamic experimental results: motor speed N, electromagnetic torque T_e, E_d and E_q of the proposed method when $R_s = 0.2R_{s0}$, $L_s = 3L_{s0}$ and $\psi_f = 2\psi_{f0}$. (a) Speed change. (b) Torque change.

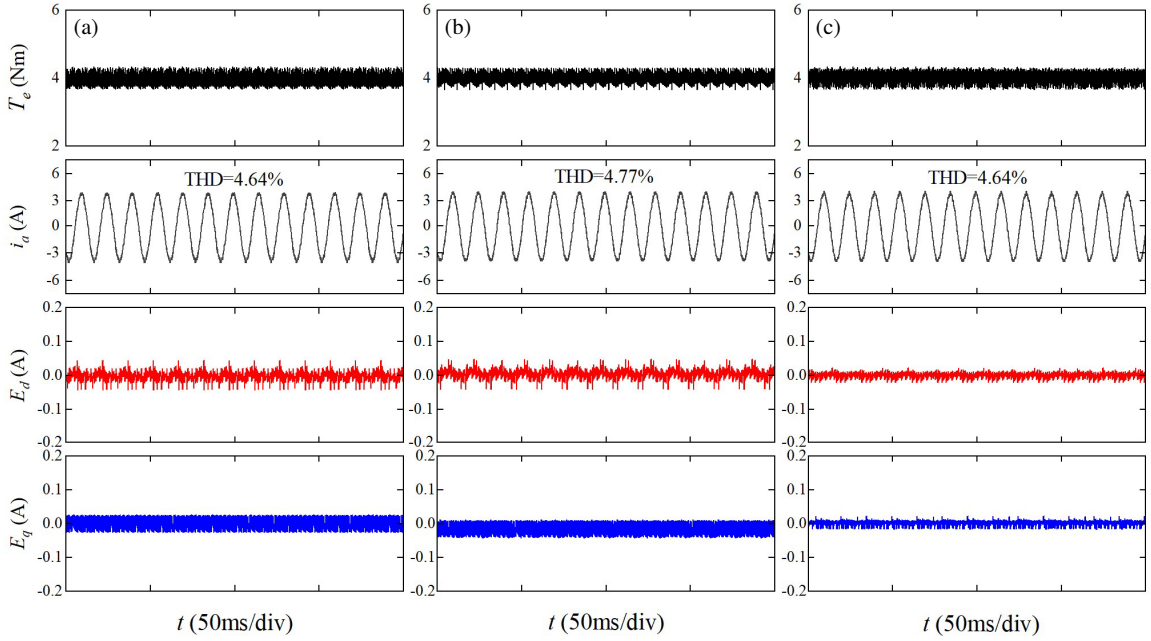

FIGURE 9. Experimental results: electromagnetic torque T_e, i_a, E_d and E_q of three methods at 1000 rpm and 4 Nm load torque when the parameters match. (a) T-MPCC. (b) LDC-MPCC. (c) The proposed method.

4 Nm load torque, and the comparison waveforms are shown in Figs. 9–11. When the parameters are not changed and matched with the actual motor parameters, the experimental waveforms of the three methods are shown in Fig. 9. Comparing the waveforms of three methods, when the parameters used in the prediction model matched with the actual parameters, all prediction errors are very small, and all steady-state performances are similar.

When the motor is operating at 1000 rpm and 4 Nm load torque, and the parameters are matched, the resistance R_s and magnet flux linkage ψ_f used in the prediction equation are suddenly changed (R_{s0} to $0.2R_{s0}$, ψ_{f0} to $2\psi_{f0}$) at the same time, and the waveforms are shown in Fig. 10. From Fig. 10(a), the sudden variations of R_s and ψ_f result in an immediate increase in the prediction error E_q in T-MPCC and a shift between the reference and the actual value of i_q. From Figs. 10(b), (c), for

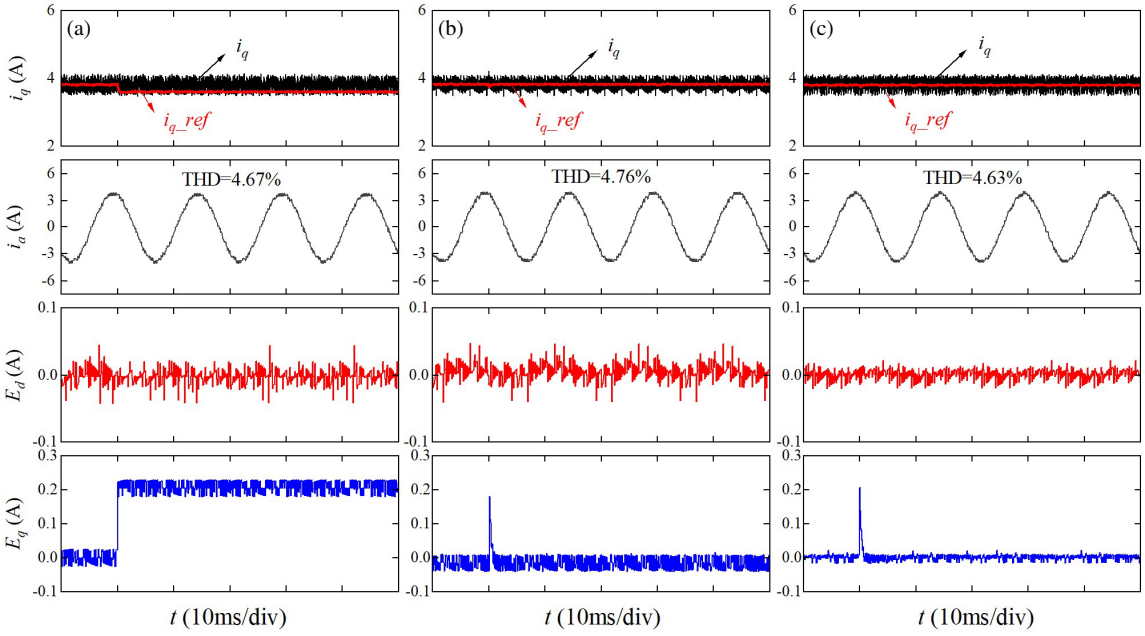

FIGURE 10. Experimental results: i_q, i_a, E_d and E_q of three methods at 1000 rpm and 4 Nm load torque when R_s and ψ_f are suddenly changed. (a) T-MPCC. (b) LDC-MPCC. (c) The proposed method.

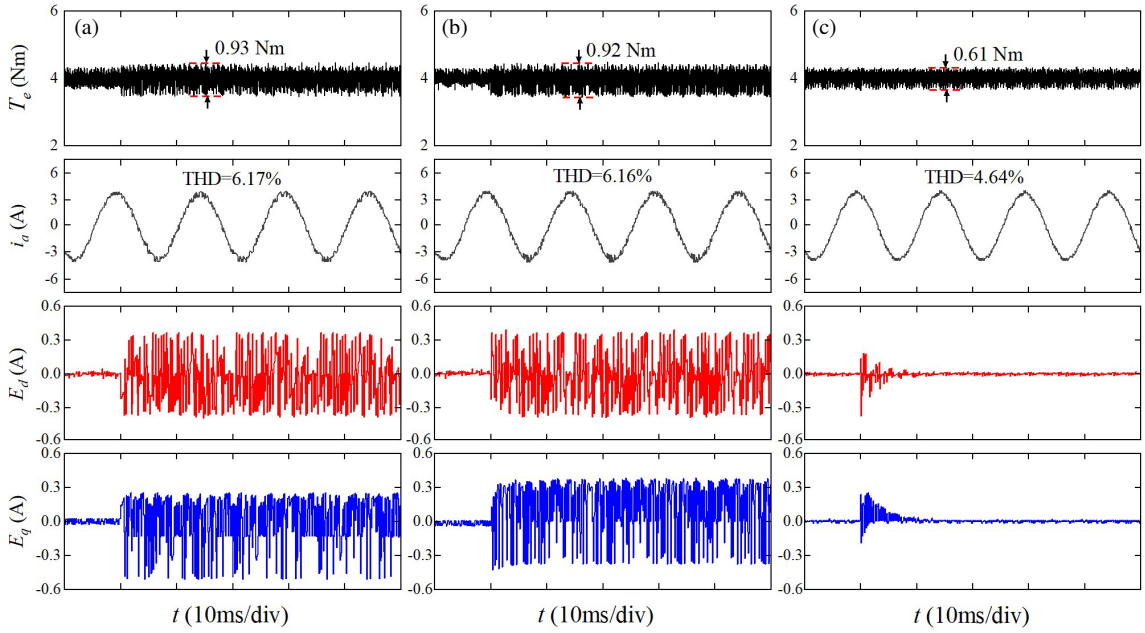

FIGURE 11. Experimental results: electromagnetic torque T_e, i_a, E_d and E_q of three methods at 1000 rpm and 4 Nm load torque when L_s is suddenly changed from L_{s0} to $3L_{s0}$. (a) T-MPCC. (b) LDC-MPCC. (c) The proposed method.

the LDC-MPCC and the proposed method, the prediction errors increase immediately at the sudden changes of R_s and ψ_f, but the compensation mechanism makes the current prediction errors converge quickly and suppresses the current static error. It should be noted that the errors caused by the mismatch of R_s and ψ_f are DC error quantities. This indicates that for the prediction error due to the mismatch of R_s and ψ_f, both the LDC-MPCC and the proposed method are able to compensate for it in time and improve the prediction accuracy. The three control methods have the same i_q ripples, indicating that the mismatch of R_s and ψ_f can only affect the current static error and not increase the i_q ripples.

When the motor is operating at 1000 rpm and 4 Nm load torque, and the parameters are matched, the synchronous inductance L_s used in the prediction equation is suddenly changed (L_{s0} to $3L_{s0}$), and the waveforms are shown in Fig. 11. From Figs. 11(a) and (b), the current prediction errors of T-MPCC and LDC-MPCC immediately increase when the inductance

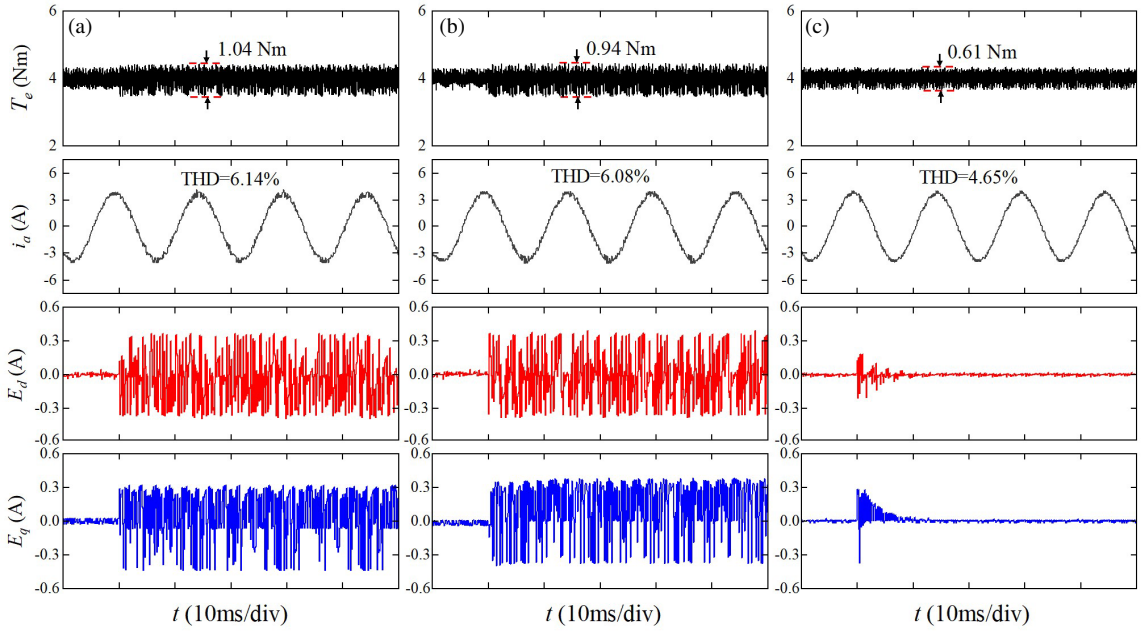

FIGURE 12. Experimental results: electromagnetic torque T_e, i_a, E_d and E_q of three methods at 1000 rpm and 4 Nm load torque when R_s, L_s and ψ_r are suddenly changed. (a) T-MPCC. (b) LDC-MPCC. (c) The proposed method.

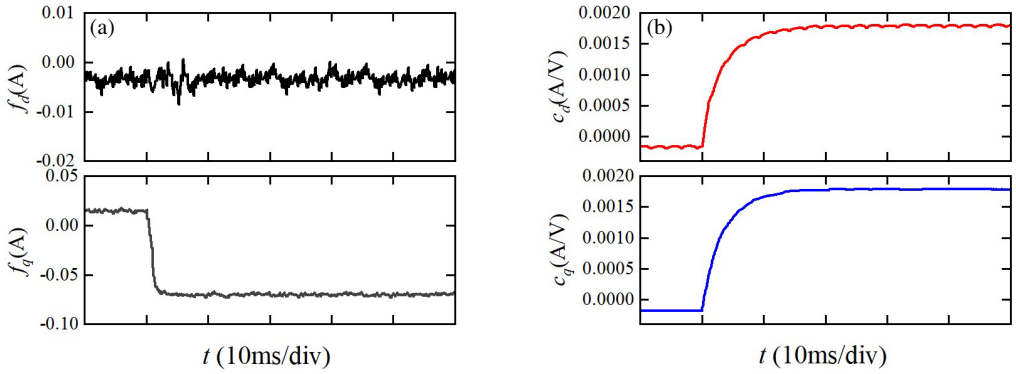

FIGURE 13. Observations of error coefficients f_d, f_q, c_d and c_q.

parameters are mismatched, and the error ripples reach 0.8 A. Meanwhile, the inductance mismatch also causes an increase in the torque ripples and stator current harmonics of both methods. The LDC-MPCC method can only compensate for the DC disturbance, and it cannot compensate for the discrete voltage-dependent disturbance. Compared to T-MPCC, LDC-MPCC merely makes the average value of the current prediction error zero, which means that the positive and negative fluctuation ranges are the same, but it cannot reduce the fluctuation range. From Fig. 11(c), the proposed method can correct prediction model through feedback compensation, which makes the current prediction error converge quickly and suppresses the deterioration of torque ripples and current harmonics.

For further verifying the dynamic regulation capability of the proposed method, R_s, ψ_f, and L_s used in the prediction equation of the normal operation motor are suddenly changed at the same time. R_s is changed from R_{s0} to $0.2R_{s0}$; ψ_f is changed from ψ_{f0} to $2\psi_{f0}$; and L_s is changed from L_{s0} to $3L_{s0}$. The experimental results are shown in Fig. 12. Similar conclusions can be reached by the closed-loop dynamic compensation mechanism, and the proposed method observes the DC quantities f_d, f_q and voltage coefficients c_d, c_q and feedback compensation, which leads to a fast convergence of the current prediction error. Fig. 13 shows the waveforms of error coefficients f_d, f_q, c_d, and c_q for this experiment, and the dynamic response of the observation system is fast and has good tracking performance. In summary, the proposed method achieves fast and stable observation with better error compensation.

5. CONCLUSION

Aiming at the parameter mismatch issue, a closed-loop control strategy for FSC-MPCC is presented in this paper. By the detailed analysis of prediction error and the fact that the lumped disturbance error compensation method cannot compensate the error related to the discrete voltage, this paper divides the current prediction error into the voltage-independent part and the voltage-dependent part. The voltage-independent part is the

DC quantity, and the voltage-dependent part is the discontinuous quantity that varies with the discrete voltage vector but whose coefficients are the DC quantities caused by the inductance mismatch. According to the different features of prediction error caused by zero and non-zero vectors, the decoupling of the two parts of prediction error is realized, and the proposed method employs two sets of proportional-integral regulators to obtain the DC components of these two parts and feeds them back into the prediction model to realize closed-loop dynamic compensation. Finally, comparative experiments verify that the proposed method can achieve good control performance and robustness under the multi-parameter mismatch condition, overcoming the drawbacks of lumped disturbance compensation.

ACKNOWLEDGEMENT

This work was supported by the Scientific Research Fund of Hunan Provincial Education Department under Grant Number 23B1017, Natural Science Foundation of Hunan Province of China under Grant Number 2022JJ50094.

REFERENCES

[1] Bi, G., Q. Wang, D. Ding, B. Li, G. Zhang, G. Wang, and D. Xu, "Multi-optimization objective online tracking-based parameter self-tuning method for sensorless PMSM drives," *IEEE Transactions on Transportation Electrification*, Vol. 9, No. 1, 1390–1402, Mar. 2023.

[2] Zhang, R., Z. Yin, N. Du, J. Liu, and X. Tong, "Robust adaptive current control of a 1.2-MW direct-drive PMSM for traction drives based on internal model control with disturbance observer," *IEEE Transactions on Transportation Electrification*, Vol. 7, No. 3, 1466–1481, Sep. 2021.

[3] Murshid, S. and B. Singh, "Implementation of PMSM drive for a solar water pumping system," *IEEE Transactions on Industry Applications*, Vol. 55, No. 5, 4956–4964, Sep.-Oct. 2019.

[4] Wei, Z., M. Zhao, X. Liu, and M. Lu, "A novel variable-proportion desaturation PI control for speed regulation in sensorless PMSM drive system," *Applied Sciences*, Vol. 12, No. 18, 9234, Sep. 2022.

[5] Wu, S., J. Zhou, X. Zhang, and J. Yu, "Design and research on high power density motor of integrated motor drive system for electric vehicles," *Energies*, Vol. 15, No. 10, 3542, May 2022.

[6] Wang, G., M. Valla, and J. Solsona, "Position sensorless permanent magnet synchronous machine drives — A review," *IEEE Transactions on Industrial Electronics*, Vol. 67, No. 7, 5830–5842, Jul. 2020.

[7] Wang, W., H. Yan, Y. Xu, J. Zou, X. Zhang, W. Zhao, G. Buticchi, and C. Gerada, "New three-phase current reconstruction for PMSM drive with hybrid space vector pulsewidth modulation technique," *IEEE Transactions on Power Electronics*, Vol. 36, No. 1, 662–673, Jan. 2021.

[8] Casadei, D., F. Profumo, G. Serra, and A. Tani, "FOC and DTC: Two viable schemes for induction motors torque control," *IEEE Transactions on Power Electronics*, Vol. 17, No. 5, 779–787, Sep. 2002.

[9] Zhang, X. and Y. He, "Direct voltage-selection based model predictive direct speed control for PMSM drives without weighting factor," *IEEE Transactions on Power Electronics*, Vol. 34, No. 8, 7838–7851, Aug. 2019.

[10] Li, T., X. Sun, G. Lei, Y. Guo, Z. Yang, and J. Zhu, "Finite-control-set model predictive control of permanent magnet synchronous motor drive systems — An overview," *IEEE/CAA Journal of Automatica Sinica*, Vol. 9, No. 12, 2087–2105, Dec. 2022.

[11] Korpe, U. U., M. Gokdag, M. Koc, and O. Gulbudak, "Modulated model predictive control of permanent magnet synchronous motors with improved steady-state performance," in *2021 3rd Global Power, Energy and Communication Conference (GPECOM)*, 67–72, Antalya, Turkey, Oct. 2021.

[12] Siami, M., D. A. Khaburi, M. Rivera, and J. Rodriguez, "An experimental evaluation of predictive current control and predictive torque control for a PMSM fed by a matrix converter," *IEEE Transactions on Industrial Electronics*, Vol. 64, No. 11, 8459–8471, Nov. 2017.

[13] Ge, L., J. Zhong, J. Huang, N. Jiao, S. Song, and R. W. D. Doncker, "A novel model predictive torque control of srms with low measurement effort," *IEEE Transactions on Industrial Electronics*, Vol. 70, No. 4, 3561–3570, Apr. 2023.

[14] Zhang, Y., D. Xu, and L. Huang, "Generalized multiple-vector-based model predictive control for PMSM drives," *IEEE Transactions on Industrial Electronics*, Vol. 65, No. 12, 9356–9366, Dec. 2018.

[15] Niu, F., X. Wang, S. Huang, X. Huang, L. Wu, K. Li, and Y. Fang, "Current prediction error reduction method of predictive current control for permanent magnet synchronous motors," *IEEE Access*, Vol. 8, 124 288–124 296, 2020.

[16] Siami, M., D. A. Khaburi, A. Abbaszadeh, and J. Rodriguez, "Robustness improvement of predictive current control using prediction error correction for permanent-magnet synchronous machines," *IEEE Transactions on Industrial Electronics*, Vol. 63, No. 6, 3458–3466, Jun. 2016.

[17] Yao, X., C. Ma, J. Wang, *et al.*, "Robust model predictive current control for PMSM based on prediction error compensation," *Proceedings of the CSEE*, Vol. 41, No. 17, 6071–6080, 2021.

[18] Türker, T., U. Buyukkeles, and A. F. Bakan, "A robust predictive current controller for PMSM drives," *IEEE Transactions on Industrial Electronics*, Vol. 63, No. 6, 3906–3914, Jun. 2016.

[19] Yuan, X., S. Zhang, and C. Zhang, "Improved model predictive current control for SPMSM drives with parameter mismatch," *IEEE Transactions on Industrial Electronics*, Vol. 67, No. 2, 852–862, Feb. 2020.

[20] Li, C., Z. Liu, X. Wu, F. He, Z. Lv, J. Li, and G. Tan, "Analysis and robustness improvement of finite-control-set model predictive current control for IPMSM with model parameter mismatches," *IEEE Access*, Vol. 10, 93 381–93 394, 2022.

[21] Wang, F., K. Zuo, P. Tao, and J. Rodríguez, "High performance model predictive control for PMSM by using stator current mathematical model self-regulation technique," *IEEE Transactions on Power Electronics*, Vol. 35, No. 12, 13 652–13 662, Dec. 2020.

[22] Zhang, X., B. Hou, and Y. Mei, "Deadbeat predictive current control of permanent-magnet synchronous motors with stator current and disturbance observer," *IEEE Transactions on Power Electronics*, Vol. 32, No. 5, 3818–3834, May 2017.

[23] Ke, D., F. Wang, L. He, and Z. Li, "Predictive current control for PMSM systems using extended sliding mode observer with Hurwitz-based power reaching law," *IEEE Transactions on Power Electronics*, Vol. 36, No. 6, 7223–7232, Jun. 2021.

[24] Wang, F., D. Ke, X. Yu, and D. Huang, "Enhanced predictive model based deadbeat control for PMSM drives using exponential extended state observer," *IEEE Transactions on Industrial Electronics*, Vol. 69, No. 3, 2357–2369, Mar. 2022.

[25] Yu, K. and Z. Wang, "Improved deadbeat predictive current control of dual three-phase variable-flux PMSM drives with composite disturbance observer," *IEEE Transactions on Power Electronics*, Vol. 37, No. 7, 8310–8321, Jul. 2022.

[26] Yang, N., S. Zhang, X. Li, and X. Li, "A new model-free deadbeat predictive current control for PMSM using parameter-free Luenberger disturbance observer," *IEEE Journal of Emerging and Selected Topics in Power Electronics*, Vol. 11, No. 1, 407–417, Feb. 2023.